ELSEVIER

Journal of Nuclear Materials 290–293 (2001) 743–747

journal of nuclear materials

www.elsevier.nl/locate/jnucmat

A 2D fluid model of the scrape-off layer (SOL) using adaptive unstructured finite volumes

Fabio Subba [a,b,c,*], Roberto Zanino [a,b]

[a] *Dipartimento di Energetica, Politecnico di Torino, C. so Duca degli Abruzzi 24, Torino 10129, Italy*
[b] *Istituto Nazionale Fisica della Materia, sez. A, Torino Politecnico, Italy*
[c] *Plasma and Energy Physics Group, Department of Theoretical Physics, University of Innsbruck, A-6020 Innsbruck, Austria*

Abstract

Recent advances in the development of adaptive grid methods for the 2D fluid simulation of tokamak edge plasmas are presented. Based on previous experiences on the solution of scalar model problems using both finite elements (FE) and finite volumes (FV), the first extension of the technique to a simplified version of the full system of Braginskii equations is presented here. The performances of adaptive grid technique are discussed and compared to the traditional fixed meshes on model problems representing a steady-state detachment and a transient evolution. © 2001 Published by Elsevier Science B.V.

PACS: 52.55.Fa; 52.40.Hf; 52.55.Dy; 52.55-y
Keywords: Fluid modeling; Tokamak; Detachment; ELM

1. Introduction

2D numerical fluid simulation of edge plasmas is a powerful, well-established tool for the design and analysis of fusion experiments. Presently, most of the codes (such as, for example, those used in [1,2]) employ structured computational grids. This allows implementing standard schemes and fast algorithms, but limits the grid flexibility. For instance, if the grid needs to be adapted by, e.g., the insertion of a new node on a structured grid, this requires adding a full line of nodes along one coordinate direction (radial or poloidal). As a consequence, some simulations may need unnecessarily many nodes. Moreover, grid adaptation is not automatic, and must be done manually. These limitations stimulated the exploration of the possibility to exploit unstructured grids, which led in the past to the exploitation of the FE approach to meet naturally the need of geometrical flexibility [3]. Some attempts to introduce local refinement have also been developed by the authors in the past using both the FE approach (see e.g., [4,5]) and the FV method [6,7]. Unstructured grids are also planned to be used in newly developed codes for machines with complex geometries like stellarators [8]. Some expertise was developed in the past solving scalar advection–diffusion–radiation problems using adaptive grids with both FE and FV methods [4,5,7]. Recently, the new adaptive grid edge multifluid code APOLLO [7] was developed, to exploit the conservation properties of FV. Here the first application of this technique to a complete set of plasma edge fluid equations (vector problem) is presented. In Section 2 the model is illustrated. Section 3 describes its application to a steady-state detachment scenario. In Section 4 a transient evolution induced by an external perturbation is studied. Finally, in Section 5 the results are resumed and some possible developments suggested.

2. Model description

The solved set of plasma equations constitutes the common basis for the most used fluid edge codes [1,2].

* Corresponding author. Tel.: +43-512 507 6220; fax: +43-512 507 2919.
E-mail address: fabio.subba@uibk.ac.at (F. Subba).

0022-3115/01/$ - see front matter © 2001 Published by Elsevier Science B.V.
PII: S0022-3115(00)00451-7

The Braginskii formulation [9] is used along magnetic field lines, while diffusive anomalous transport is assumed in the radial direction (perpendicular to the field). The neutral particles are described by a diffusive model and interact with the plasma via recycling, ionization and recombination processes. For the time being, charge-exchange is neglected. Orthogonal Cartesian coordinates are used, where (x) represents the poloidal direction and (y) the radial. The equations are:

$$\frac{\partial n}{\partial t} + \nabla \cdot (n\bar{u}) = S^n_{\text{ion}} + S^n_{\text{rec}}, \tag{1}$$

$$u_y = -\frac{D_n}{n}\frac{\partial n}{\partial y}, \tag{2}$$

$$\frac{\partial \Gamma_x}{\partial t} + \nabla \cdot \left(\Gamma_x \bar{u} - \hat{\eta}^i \cdot \nabla u_x + (p_{\text{i}} + p_{\text{e}})\bar{e}_x\right) = S^{\Gamma_x}_{\text{rec}}, \tag{3}$$

$$\begin{aligned}\frac{\partial}{\partial t}\left(\frac{3}{2}nT_{\text{e}}\right) + \nabla \cdot \left(\frac{5}{2}nT_{\text{e}}\bar{u} - \hat{\kappa}^{\text{e}} \cdot \nabla T_{\text{e}}\right) \\ = -k(T_{\text{e}} - T_{\text{i}}) + \bar{u} \cdot \nabla p_{\text{e}} + S^{E_{\text{e}}}_{\text{ion}} + S^{E_{\text{e}}}_{\text{rad}} + S^{E_{\text{e}}}_{\text{rec}},\end{aligned} \tag{4}$$

$$\begin{aligned}\frac{\partial}{\partial t}\left(\frac{3}{2}nT_{\text{i}} + \frac{1}{2}nmu_x^2\right) + \nabla \cdot \left(\left(\frac{5}{2}nT_{\text{i}} + \frac{1}{2}nmu_x^2\right)\bar{u}\right. \\ \left. - \left(\hat{\kappa}^i \cdot \nabla T_{\text{i}} + \frac{1}{2}\hat{\eta}^i \cdot \nabla u_x^2\right)\right) \\ = k(T_{\text{e}} - T_{\text{i}}) - \bar{u} \cdot \nabla p_{\text{e}} + S^{E_{\text{i}}}_{\text{ion}} + S^{E_{\text{i}}}_{\text{rec}},\end{aligned} \tag{5}$$

$$\frac{\partial N}{\partial t} - \nabla \cdot (D_N \nabla N) = S^N_{\text{ion}} + S^N_{\text{rec}}. \tag{6}$$

Eqs. (1)–(6) state, respectively: conservation of plasma density n, a diffusive ansatz for the radial velocity u_y, conservation of the parallel component $\Gamma = nmu_x$ of the plasma momentum (m ion mass, u_x parallel velocity), of the electron energy, of the ion energy and of the neutral atom density N, respectively. Pressures are related to plasma density and temperatures via $p_{\text{e,i}} = nT_{\text{e,i}}$. The ion parallel viscosity $\eta^{\text{i}}_{\parallel}$ and the parallel thermal conductivities $\kappa^{\text{e,i}}_{\parallel}$ follow from Braginskii [9], while the radial coefficients are anomalous. The thermal coupling coefficient k comes from Braginskii too, and the plasma and neutral diffusivities (D_n and D_N) are assumed constant. $S^{n,N}_{\text{ion}}$ and $S^{n,N}_{\text{rec}}$ are external sources for plasma and neutral particles due to ionization and recombination, $S^{\Gamma_x}_{\text{rec}}$ the recombination parallel momentum sink, $S^{E_{\text{e}}}_{\text{rad}}$ the electron energy sink due to radiation processes, and $S^{E_{\text{e}},E_{\text{i}}}_{\text{ion}}$ and $S^{E_{\text{e}},E_{\text{i}}}_{\text{rec}}$ are the ionization and recombination energy sources (sinks) for ions and electrons. The form of the external sources varies according to the case studied, and will be specified later.

Eqs. (1)–(6) are solved on the rectangle $(x, y) \in (0, 2) \times (0, 0.02)$ (units are in meters). Side $x = 2$ represents the divertor plate. Side $y = 0$ is split in two tracts: $x < 1.4$ m (main plasma) and $1.4 < x < 2$ m (private flux region). The external radial boundary is set arbitrarily at $y = 2$ cm (i.e., deep enough radially to include the relevant physical effects of the model, which extend for a few millimeters). Finally, $x = 0$ is a symmetry boundary. Conditions are set as follows: sheath conditions are imposed at the plate, symmetry conditions at the private flux boundary and at $x = 0$, zero radial derivatives and parallel momentum at $y = 2$ cm. At the main plasma interface, either temperatures and density or particle and energy fluxes are imposed.

3. Detachment simulation

First a detachment is simulated. The recycling coefficient is set at $R = 0.99$ and ionization, recombination and radiation processes are included. The ionization particle source is $S^n_{\text{ion}} = -\langle\sigma V\rangle_{\text{ion}} nN$ (reaction rates data are from Wesson [10]). The radiation energy source is $S^{E_{\text{e}}}_{\text{rad}} = -\langle\sigma V \varepsilon\rangle \xi n^2$: a constant impurity fraction $\xi = 3 \times 10^{-2}$ is assumed and reaction rates data are taken from Bonnin et al. [11]. For each ionization event 30 eV are extracted from the electrons, and the energy of a thermal particle is added to the ions (i.e., neutrals are in thermal equilibrium with the plasma). For each recombination, the energy corresponding to a thermal electron and ion, and the momentum of a thermal ion are extracted. The plasma diffusion coefficient is $D_n = 0.125$ m^2 s^{-1}. Some parameters in the neutral model are chosen ad hoc: the diffusion coefficient $D_N = 10^2 D_n$ and the recombination source $S^{\text{s}}_{\text{rec}} = -f(T_{\text{e}})n^2$, with the recombination rate $f(T_{\text{e}}) = 10^2 \times (3 - T_{\text{e}})$ for $T_{\text{e}} < 3$ eV, while $f(T_{\text{e}}) = 0$ otherwise.

An efficient way to adapt the grid, in steady-state simulations, is to get first a rough solution, and then to allow for successive adaptations. Each cell may be independently refined or coarsened. When a cell is refined, its refinement level is said to increase. The refinement criterion is based on an evaluation of the second derivatives of the estimated solution in scalar cases [4,5]. Here, there is the additional task to choose a subset of the dependent variables on which the adaptivity criterion should be based. Numerical experiments show that it is necessary to check at least both plasma and neutral density to get an accurate solution.

Fig. 1 shows parallel profiles of plasma density on the lower separatrix near the plate, on different grids. Four successive refinement levels are enough to converge. Notice the decrease near the target on the finest grids. It goes together with a reduction of the input power fraction reaching the plate (45% on the coarsest grid, 29% on the finest). This effect is due to the onset of recombination, which is not seen on the coarsest grid because the electron temperature stays always above the cut-off (3 eV), but captured on the more refined grids (the

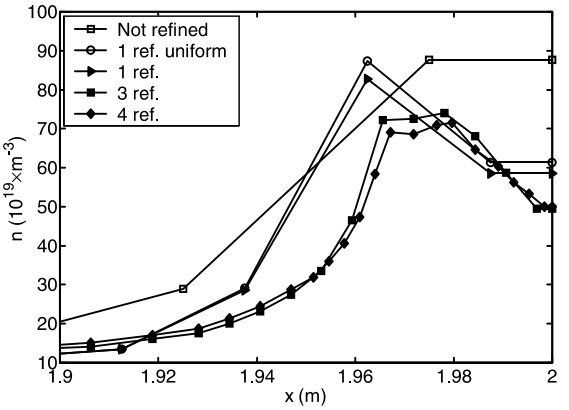

Fig. 1. Plasma density profiles $x = 0$ in the target region on four increasingly refined grids. The drop in plasma density on the finest grids is due to recombination, active for $T_e < 3$.

maximum T_e at the divertor drops from 3.2 eV on the coarsest grid to 2.7 on the finest). As each uniform refinement increases the total number of nodes by a factor 4, and the required CPU time by (at least) the same amount, the finest uniform grid practically affordable for us corresponds to one refinement level, which is still too rough to catch the source details.

Fig. 2 shows a zoom of the neutral density contours near the plate, and the grid in the same region. The successive refinements structure is clearly visible. The refinement between $x = 1.95$ and $x = 1.97$ is due to the interaction with the ionization source (not shown in the figure). The coarsest cells in the picture belong to the first refinement level. Four of them grouped together form a cell of the zeroth level, which cover almost completely the remaining part of the domain (not shown).

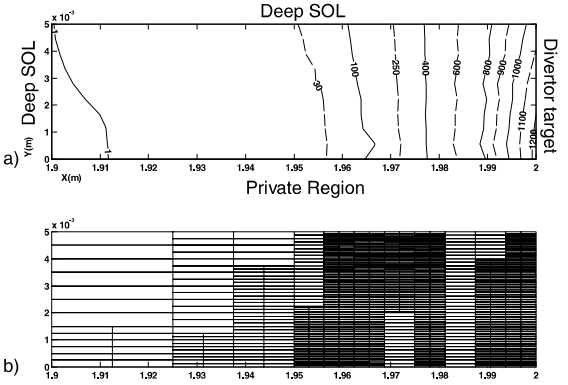

Fig. 2. (a) *Zoom* of the neutral density near the divertor. (b) The finest computational grid used: the successive refinements structure is seen. The refinement in the region $1.95 < x < 1.97$ is due to the ionization particle source.

Table 1
Normalized CPU time required by the solution of the discretized version of (1)–(6) for the detachment simulation on six different grids

Grid type	Nodes	CPU time
Not refined (structured)	924	1.00
1 refinement, uniform	3696	4.55
1 refinement, adaptive	1185	1.70
2 refinements, adaptive	1719	2.49
3 refinements, adaptive	3177	4.66
4 refinements, adaptive	5985	14.06

It is interesting to discuss now the performances of adaptive grids in terms of memory and CPU time required. The memory needed is proportional to the number of nodes. The computational time is also influenced by the grid structure. In fact, the discretized form of (1)–(6) is a set of coupled algebraic equations to be solved simultaneously. Generally, solver performances are influenced by the matrix properties, which reflect the grid structure. As a consequence, solver speed will likely decrease on unstructured grids. Table 1 compares the CPU time spent solving algebraic systems on the different grids of Fig. 1. The CPU time required per cell increases rapidly on the unstructured meshes. Nonetheless, adaptivity allows a considerable gain at an equal refinement level: 1 adaptive refinement needs only about 1/3 of the nodes and CPU time of one uniform refinement, still Fig. 1 shows that both give very close results of comparable accuracy. Finally, it is important to notice that three adaptive refinements still have about the same number of nodes as one uniform refinement, but they give an almost converged solution, while one uniform refinement does not (see Fig. 1).

4. Perturbation-induced transient

Performances of adaptive grids on transient processes are studied by simulating the evolution of a density perturbation. This is excited injecting a burst of particles from the main plasma for 0.05 ms in the region $0.6\ \text{m} \leqslant x \leqslant 1.2\ \text{m}$. During the burst, the imposed input particle flux from the main plasma integrated toroidally raises from 7.75×10^{22} up to $5.425 \times 10^{23}\ \text{m}^{-1}\ \text{s}^{-1}$. All the injected particles have a temperature of 100 eV. This technique could also be applied, for example, to the simulation of an ELM event [12]. The induced transient is followed for 0.1 ms. (This duration is not sufficient to bring the system completely back to steady state, but the most intense phenomena during the transient take place in its initial stages, and adaptivity performances were tested without increasing unnecessarily the run duration). As the action of sources generally causes many phenomena in the divertor region which could make

more difficult the analysis of the simulations, they are switched off and no neutrals are assumed.

Adaptive study of transient processes presents additional features with respect to steady-state problems. The grid must change often enough to follow the system evolution. However, the interpolation involved in the adaptation introduces pulsed disturbances that must be minimized. Moreover, frequent interpolations introduce some numerical diffusivity, which is dangerous especially in convection-dominated problems [5]. It is useful to define the parameter $\Delta_k = \langle (n_k - n_0)/n_k \rangle$, where n_0 is the first value of the plasma density obtained on the present grid, n_k is the density after k time steps and $\langle \cdot \rangle$ indicates space averaging. It is found experimentally acceptable to update the grid when Δ_k becomes $> 10^{-2}$. In any case, once a new grid is created it is not changed for at least 40 time steps. Once the necessity of a grid adaptation has been detected, the actual refinement/coarsening criterion is again that used in Section 3, with the difference that now the function checked is the plasma density (see [4] for more details).

Fig. 3 shows the evolution of the maximum plasma density in the SOL, induced by the perturbation in the particle influx. All the shown runs start on the same initial uniform grid, but the number of refinement levels allowed during the evolution is different. As the difference between the last two curves (two and three refinement levels at most, respectively) is less than 10%, it is accepted as a spatially converged solution.

Fig. 4 shows the grid history of the converged simulation of Fig. 3. Notice that the number of nodes increases temporarily during the violent period of the transient and decreases later (minimum is 924 nodes, maximum 3399 and time-averaged value 2278). Finally, Fig. 5 shows the density contours for the same run,

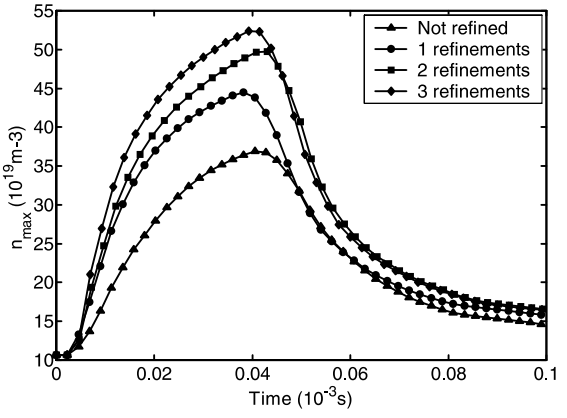

Fig. 3. Evolution of the maximum density on different grids. The lower curve (triangles) corresponds to a structured uniform grid with 40 poloidal and 20 radial nodes. Circles, squares and diamonds show the same transient followed on adaptive grids with at most 1, 2 and 3 refinement levels.

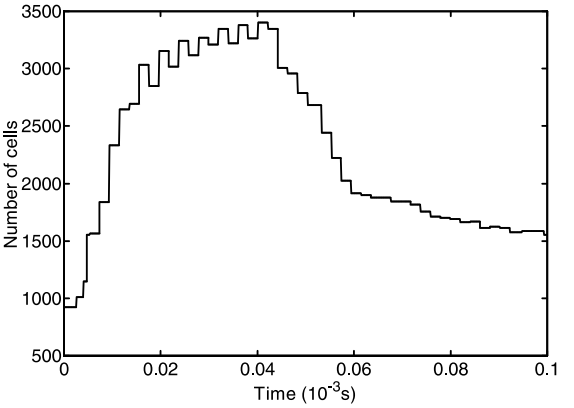

Fig. 4. Evolution of the number of nodes for the most accurate run of Fig. 3 (three refinements at most).

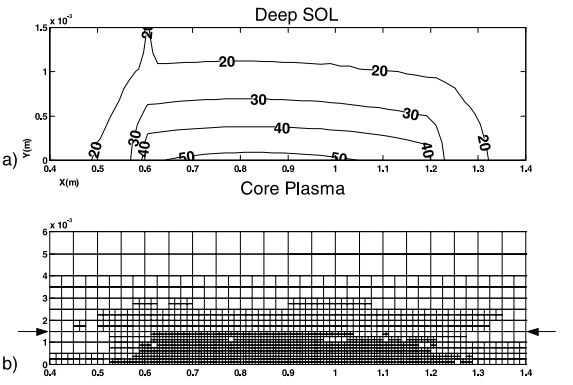

Fig. 5. (a) *Zoom* of the density contour at $t = 4.01 \times 10^{-5}$ s. (b) The relative unstructured adapted grid. Notice a different zoom in y has been used to better appreciate the grid structure. The arrows mark the region to which the contour in (a) refers.

taken at $t = 4.01 \times 10^{-5}$ s, and the relative grid, which follows closely the density pattern.

5. Conclusions

The first application of adaptive unstructured grids to a full set of model equations for the fluid simulation of the edge plasma in fusion devices was presented. The method was applied to steady-state and transient problems, and compared with results obtained on traditional structured fixed grids. For the cases considered here adaptive grids perform better than the traditional ones, due to the reduced number of nodes needed for the same accuracy level.

In the future, it is desirable to abandon the simplifications still present in the model: rectangular geometry

and reduced physics. In particular, extension of the present strategy to realistic curvilinear geometry should not involve any principal difficulties. Other improvements are also possible (especially related to fast and efficient mesh control strategy) to further enhance the effectiveness of unstructured adaptive grids as a plasma fluid-modeling tool.

References

[1] T.D. Rognlien et al., J. Nucl. Mater. 266–269 (1999) 654.
[2] D.P. Coster, K. Borrass, R. Schneider et al., J. Nucl. Mater. 266–269 (1999) 804.
[3] R. Zanino, J. Comput. Phys. 138 (1997) 881.
[4] R. Zanino, F. Subba, Contrib. Plasma Phys. 38 (1998) 355.
[5] R. Zanino, G. Belgiorno, F. Subba, Czechoslovak J. Phys. 48 (1998) 351.
[6] O.V. Batishchev, A.A. Batishcheva, A.S. Kholodov, J. Plasma Phys. 61 (1999) 701.
[7] F. Subba, PhD thesis, Politecnico di Torino, Turin, Italy, 1999.
[8] M.A. Borchardt, A. Mutzke, J. Nuhrenberg, J. Riemann, R. Schneider, in: B. Schweer, G. VanOost, E. Vietzke (Eds.), Proceedings of the 26th EPS Conference on Controlled Fusion and Plasma Physics, ECA 23J, Maastricht, 1999, p. 1501.
[9] S.I. Braginskii, in: M.A. Leontovich (Ed.), Transport Processes in a Plasma, Reviews of Plasma Physics, Consultants Bureau, New York, 1965, p. 205.
[10] J. Wesson, Tokamaks, Clarendon, Oxford, UK, 1987.
[11] X. Bonnin et al., in: Atomic and Plasma-Material Interaction Data for Fusion, supplement to the J. Nucl. Fus. 2 (1992) 117.
[12] D.L. Hillis et al., J. Nucl. Mater. 266–269 (1999) 1084.